JOURNAL OF GEOPHYSICAL RESEARCH, VOL. 99, NO. D5, PAGES 10,319–10,332, MAY 20, 1994

Evaluation of the SKYHI general circulation model using aircraft N_2O measurements 2. Tracer variability and diabatic meridional circulation

S. E. Strahan[1]

Atmospheric and Oceanic Sciences Program, Princeton University, Princeton, New Jersey

J. D. Mahlman

NOAA Geophysical Fluid Dynamics Laboratory, Princeton, New Jersey

Abstract. Winter polar stratospheric nitrous oxide (N_2O) measurements made during two NASA polar aircraft field campaigns provide a unique opportunity to evaluate the performance of the 1° latitude resolution version of the Geophysical Fluid Dynamics Laboratory's "SKYHI" general circulation model. This high-resolution model has been integrated 20 months, producing one Antarctic and two Arctic winters. Power spectra of the dynamically controlled tracer N_2O are used as a diagnostic of wave activity. Comparison of the spectra of SKYHI and the observations shows that the SKYHI Arctic winter lower stratosphere is dynamically active enough to generate realistic mesoscale tracer variability but that the SKYHI Antarctic has deficient variability at scales of 220-3000 km. Low-pass filtering is applied to a new type of analysis that attempts to discriminate between different sources of atmospheric variability, to the extent that different sources are characterized by different timescales. The goal is to diagnose mesoscale sources of tracer variability in the model and in the observations and then to assess whether SKYHI generates variability for the right physical reasons. This analysis shows that variability from "slow" processes such as planetary wave breaking dominates and is generated in realistic amounts in the SKYHI Arctic winters. The SKYHI Antarctic vortex shows insufficient "debris" from planetary wave breaking at scales below 700 km. The balance between diabatic descent inside the vortex and wave breaking in the "surf zone" generates N_2O gradients at the vortex edge in the model and the real atmosphere. Because the diabatic circulation is driven by wave activity, the strength of model wave activity diagnosed by the spectral analysis and the mean N_2O gradients can be used to evaluate SKYHI's diabatic circulation and net tracer transport. In the Arctic, SKYHI temperatures, spectral results, and realistic N_2O gradients at the vortex edge suggest a reasonable diabatic meridional circulation and transport. Antarctic spectral results, low vortex temperatures, and flatter N_2O gradients at the edge all support the conclusion that the diabatic circulation and wave activity in the model southern hemisphere is too weak.

1. Introduction

In the companion paper [*Strahan and Mahlman*, this issue] (hereafter referred to as part 1), polar lower stratospheric N_2O measurements made as part of two NASA field campaigns were compared with N_2O fields from the high-resolution Geophysical Fluid Dynamics Laboratory's (GFDL) SKYHI general circulation model (GCM). Measurements of this conservative tracer, obtained both inside and outside of both winter polar vortices [*Podolske et al.*, 1989; *Loewenstein et al.*, 1990], illustrate descent and comparative isolation of air inside the Arctic and Antarctic vortex. In part 1, comparison of the measurements with the GFDL SKYHI GCM showed similar descent and isolation in the model's Arctic vortex but indicated a circulation in the model Antarctic stratosphere that was too weak. These conclusions were supported by reasonable temperatures in the SKYHI Arctic lower stratosphere and by too low temperatures inside the SKYHI Antarctic vortex (part 1). While the mean N_2O fields derived in part 1 are very useful in diagnosing air motions in and around the vortex, the Airborne Antarctic Ozone Experiment (AAOE) and Airborne Arctic Stratospheric Expedition (AASE) data sets used to derive those means also contain a good deal of information on atmospheric variability. These data sets provide an unprecedented opportunity for evaluating the detailed transport characteristics of a uniquely high resolution general circulation model.

The power spectrum of the dynamically controlled tracer N_2O is a measure of atmospheric variability as a function of scale and as such it can be used as a diagnostic of wave activity. Variability here is defined as deviation from the seasonal mean which has been estimated from the flight data (part 1). To calculate the power spectrum, the mean is removed from the isentropic flight data, the Fourier transform (FT) of the N_2O residual is computed, and the square of the resulting

[1]Now at Applied Research Corporation, Landover, Maryland.

Paper number 94JD00044.
0148-0227/94/94JD-00044$05.00

Fourier coefficients produces the power spectrum. Both the slope and the amplitude of the resulting power spectrum yield information on variability. The spectral slope is an integral measure of the balance between the production of variance at different spatial scales, the rate at which large-scale variations are cascaded into smaller-scale variations, and how fluctuations are removed by turbulence and diffusion. In this paper, power spectra of simulated flights through the 1° latitude version of the SKYHI GCM will be compared with spectra calculated from AASE and AAOE aircraft observations. This comparison provides the first opportunity to evaluate whether this uniquely high resolution model has realistic small-scale variability, i.e., whether the model has sufficient wave activity to generate variability matching the observations. Comparison of the spectral slopes also provides a direct test of parameterized subgrid scale diffusion in SKYHI, because the model's spectral slope is partly determined by the parameterization.

A new application of spectral analysis is presented that extends the diagnostic capabilities of the power spectra comparison. This analysis attempts to discriminate between different sources of variability, such as planetary wave and gravity wave breaking, to the extent that these processes are characterized by different timescales. Because wave activity drives the diabatic circulation, the diagnosis of wave activity from the spectral analyses presented here, supported by the mean tracer fields and climatologies discussed in part 1, allows an evaluation of the diabatic meridional circulation and tracer transport in the stratosphere of the SKYHI GCM.

2. Power Spectral Analysis as a Diagnostic for Variability

AASE and AAOE data sets used in this calculation are described in part 1. Only flight segments on isentropic surfaces are used in this analysis; there are 38 segments of ~1000 km for AASE and 31 ~1000-km segments for AAOE. Information about longer scales is obtained by performing the calculation with 1700-km segments, but with only 12 flight segments of that length available for each hemisphere; the statistical significance of these results is thus limited. For both SKYHI Arctic winters, power spectra of model output are calculated from 25 days (from mid-December to the end of January), using four longitudes between 3° and 19°E (Scandinavia) and four isentropic surfaces from 420 to 480 K. SKYHI Antarctic spectra are calculated in an analogous way using 25 days (from mid-August to early October) and four longitudes near the Palmer peninsula (280°-300°E). The spatial and temporal characteristics of the model data sets were chosen to match the observations. Latitudes from 50° to 89° were chosen to extend the wavelength range covered by the calculation. To calculate power spectra for both the observations and the model "flight data," the seasonal mean is first removed. These means are shown in Plates 1 and 2 of part 1. The mean subtracted from each flight segment is in accordance with the isentropic surface and latitude range (with respect to the vortex edge) of that flight. Because the flight observations are not continuous but have a 2-min calibration gap every 11.5 min, a continuous record is created for the FT by linear interpolation across these gaps.

It is desirable to optimize the statistical significance of the results by maximizing the amount of flight data that can be included in the calculation. Therefore power spectra of 1000-km segments are chosen for the calculation, and the results for AASE and AAOE are shown in Figure 1. Both spectra show an approximate -5/3 to -2 slope, and total power in the Arctic is 2-3 times the Antarctic. A slope of -5/3 is expected for winds and tracers based on a quasi-two-dimensional turbulence theory [*Gage and Nastrom*, 1986; *Nastrom et al.*, 1986]. At scales greater than 100 km the difference in power between the hemispheres is statistically significant. Using the original 1.0-s resolution flight data (equivalent to 200-m spatial resolution), power spectra can be calculated down to wavelengths of 400 m. This is done using the 9.5-min segments of continuous data (the time between instrument calibration gaps), which equal ~110 km of aircraft travel. Over 400 110-km segments were available from each of the AASE and AAOE data sets. The average power spectrum for each hemisphere showed a -5/3 to -2 slope down to scales of ~500 m, with a white noise spectrum below this scale presumably due to instrument noise.

Because the ER-2 cannot fly precisely on an isentropic surface, the aircraft flight track relative to the isentropic surface introduces variability into the tracer measurements from vertical gradients of the tracer. (Put another way, adiabatic vertical displacements of air parcels along the flight track (gravity wave oscillations) prevent the ER-2 from flying on a perfectly isentropic surface.) Thus AASE and AAOE power spectra contain an additional source of variability not present in the SKYHI spectra, which are calculated unambiguously on isentropic surfaces. Aircraft deviations from isentropic flight are generally small (e.g., ± 5 K), so this

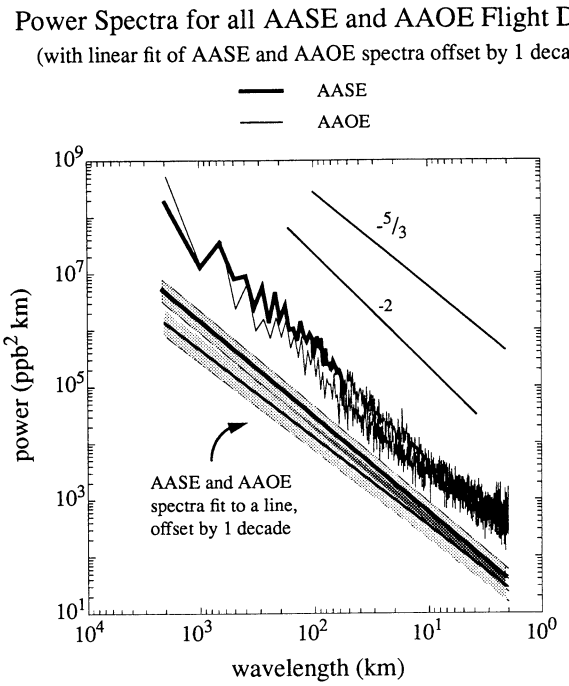

Figure 1. N_2O Power spectra for AASE and AAOE. AASE spectrum is the average of the Fourier transforms of 38 1000-km flight segments; the AAOE spectrum is the same except using 31 segments. The spectra shown were fit to a line, and these lines are plotted with a one decade offset. The shaded areas represent the 95% confidence intervals for the fitted lines. The AASE spectrum has more power than the AAOE spectrum, statistically significant at scales greater than 100 km. Below 10 km the unfitted spectra are largely overlapping.

comparison is still useful as a coarse diagnostic of tracer variability in the model. The size of this contribution to the power spectrum and a method to eliminate the contribution are discussed in the next section.

To maximize the scale overlap between model and aircraft power spectra, the spectra of 1700-km-long isentropic flight legs are computed, although this results in only 12 flight segments each available for the AASE and AAOE calculations. Figure 2 shows the results of the spectral calculations for AASE and the second SKYHI Arctic winter (AWII). In the Arctic the agreement of slopes and amplitudes is outstanding; the SKYHI results lie completely within the 95% confidence intervals of the AASE results. To first order, this implies that the SKYHI Arctic winter lower stratosphere is dynamically active enough to generate tracer variability comparable to the real atmosphere. The -5/3 to -2 slope of the SKYHI spectrum indicates that the dimensionless coefficient of the Smagorinsky nonlinear diffusion parameterization is in a proper range [*Andrews et al.*, 1983]; that is, the subgrid scale diffusion in the model is diffusing away smaller-scale features at an appropriate rate. The comparison of AASE and the first SKYHI Arctic winter (AWI) spectra (not shown) is nearly identical to Figure 2.

In Figure 3 the comparison between AAOE and the SKYHI Antarctic winter is not nearly so favorable. There is good

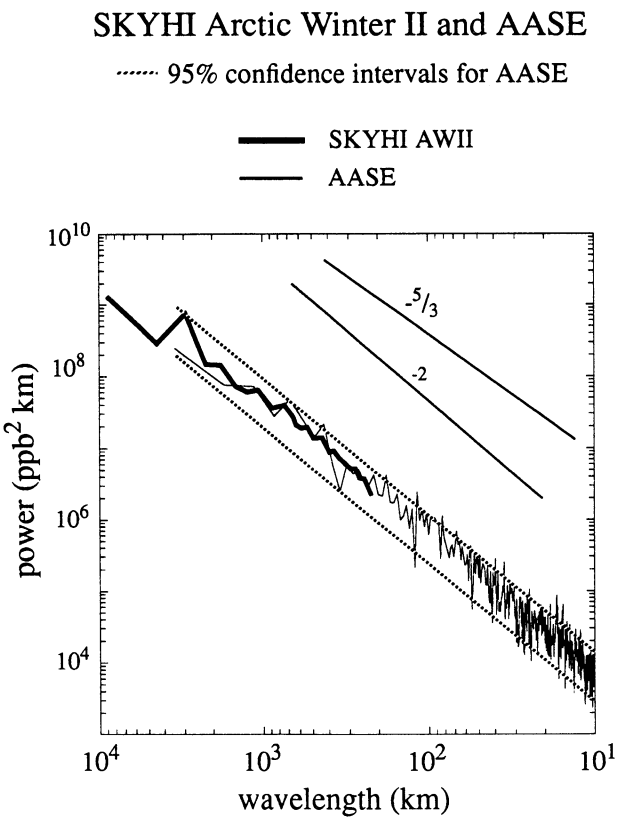

Figure 2. AASE N_2O power spectrum calculated from 12 long (1700 km) flight legs and comparison with SKYHI Arctic winter II (AWII). The 95% confidence interval for the AASE spectrum is given by the dashed lines. The SKYHI confidence interval is very narrow (±9%) and is not shown. There is excellent agreement between the model and observations. The SKYHI spectrum has a best fit slope of -1.8 and the AASE best fit slope is -1.9.

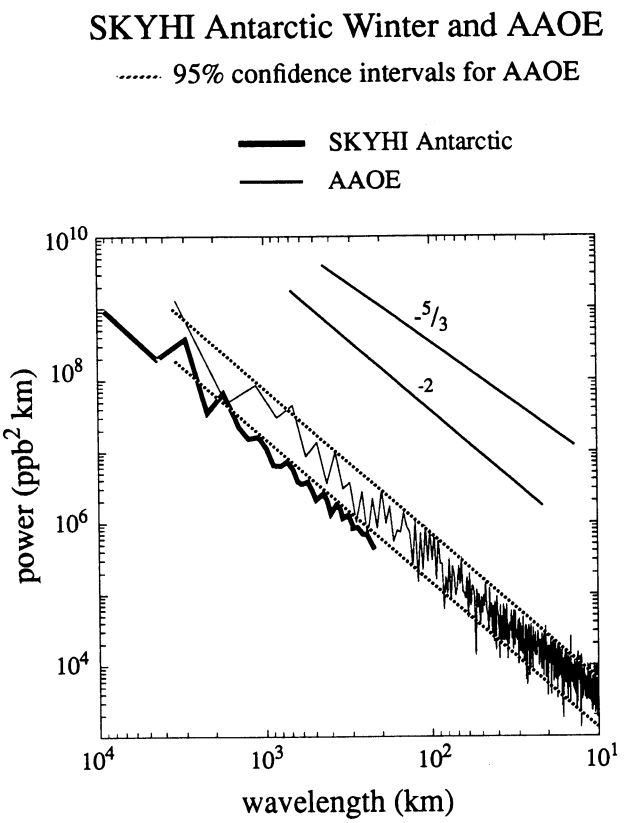

Figure 3. AAOE N_2O power spectrum calculated from 12 long (1700 km) flight legs and comparison with SKYHI Antarctic winter. The 95% confidence interval for the AAOE spectrum is given by the dashed lines. The SKYHI confidence interval is very narrow (±9%) and is not shown. Antarctic SKYHI shows less variability (power) than the Antarctic measurements. Both the SKYHI and the AAOE spectra have a best fit slope of -2.0.

agreement of the slopes, but throughout the entire range of overlap the model spectrum falls short of the AAOE spectrum by factors of 2-4 and the SKYHI results lie completely below the AAOE 95% confidence interval. In light of the model 50-mbar temperatures at 80°S that are too low by about 7 K (part 1), it is not surprising to find a shortage of dynamical activity in a model region that is too close to radiative equilibrium. It should be noted, however, that the aircraft power spectra contain small amounts of variance produced by aircraft motions (deviations from isentropic flight) and thus are not precisely comparable to the model spectra.

Separation of the Spectrum

The power spectrum is a useful measure of atmospheric variability, but it does not provide unique insight into the processes generating the variability. Some of the variability is caused by planetary wave breaking events which, for example, shear off "blobs" of air from the vortex, allowing them to be advected to lower latitudes, while wind shear stretches the parcels out to ever smaller scales until turbulent mixing and diffusion dissipate them. Other major sources of variability are gravity wave breaking and gravity wave oscillations. Gravity wave (buoyancy) oscillations are a nearly adiabatic displacement of an air parcel and therefore should tend to be

nearly "transparent" on isentropic surfaces. These processes act on different timescales: a large-scale wave breaking event may last several days, with the "debris" from the wave breaking only slowly being deformed and advected away, while gravity waves have periods on the order of hours in the lower stratosphere.

On a flight day where the two flight legs cover the same latitude, longitude, and potential temperature coordinates, one sees large features in both flight legs that are nearly identical but also many small-scale features having no correlation between the two legs. Plate 1a illustrates the similarities between northbound and southbound legs that cover the same coordinates. AASE and AAOE flight tracks are mostly meridional and sample air that is moving approximately zonally at 20-50 m/s. Thus the outbound and the return flight legs will not sample exactly the same air mass. However, it is clear from Plate 1 that there are features that remain relatively constant for several hours. (The time lag between when a particular coordinate is sampled outbound and inbound varies from as little as ~40 min to as much 5 hours.) Variance in the flight data generated by aircraft deviations from an exact isentropic surface is removed by extrapolation to a single isentropic surface. Details of this method are given at the end of this section.

Plate 1b shows how much northbound and southbound flight legs (N_i and S_i) can have in common. By removing the mean from each leg consisting of i measurements and then summing the residuals (N_i' and S_i'), the result is an "average" flight leg that retains the common features of the individual flight legs while reducing by a factor of $\sqrt{2}$ the signal that is uncorrelated between the legs. Conversely, when subtracting the residual of one flight leg from the other ($N_i' - S_i'$), the features common to both legs are removed and there is again a $\sqrt{2}$ reduction in the uncorrelated signal. These are the sum and difference time series, and their power spectra contain information on sources of atmospheric variability to the extent that different sources of variability are characterized by different timescales. The spectrum of the sum time series ($N_i' + S_i'$) consists primarily of power from "slow events" (e.g., large-scale wave breaking), while the spectrum of the difference ($N_i' - S_i'$) lacks the contribution from slowly evolving features but has power from processes with much shorter timescales. The slowly varying features common to the two legs can roughly be characterized as debris from planetary wave breaking events, and their power spectrum (which is part of the spectrum of $N_i' + S_i'$) will be arbitrarily referred to as the planetary wave debris (PWD) spectrum. The power spectrum of the difference ($N_i' - S_i'$) will be referred to arbitrarily as the random phase, or non-PWD spectrum. The random phase power is only reduced, not removed in the $N_i' + S_i'$ spectrum, with the amount of random phase power remaining equal to the power in the difference spectrum ($N_i' - S_i'$). Thus the power from planetary wave debris alone is

$$[FT(N_i' + S_i')]^2 - [FT(N_i' - S_i')]^2.$$

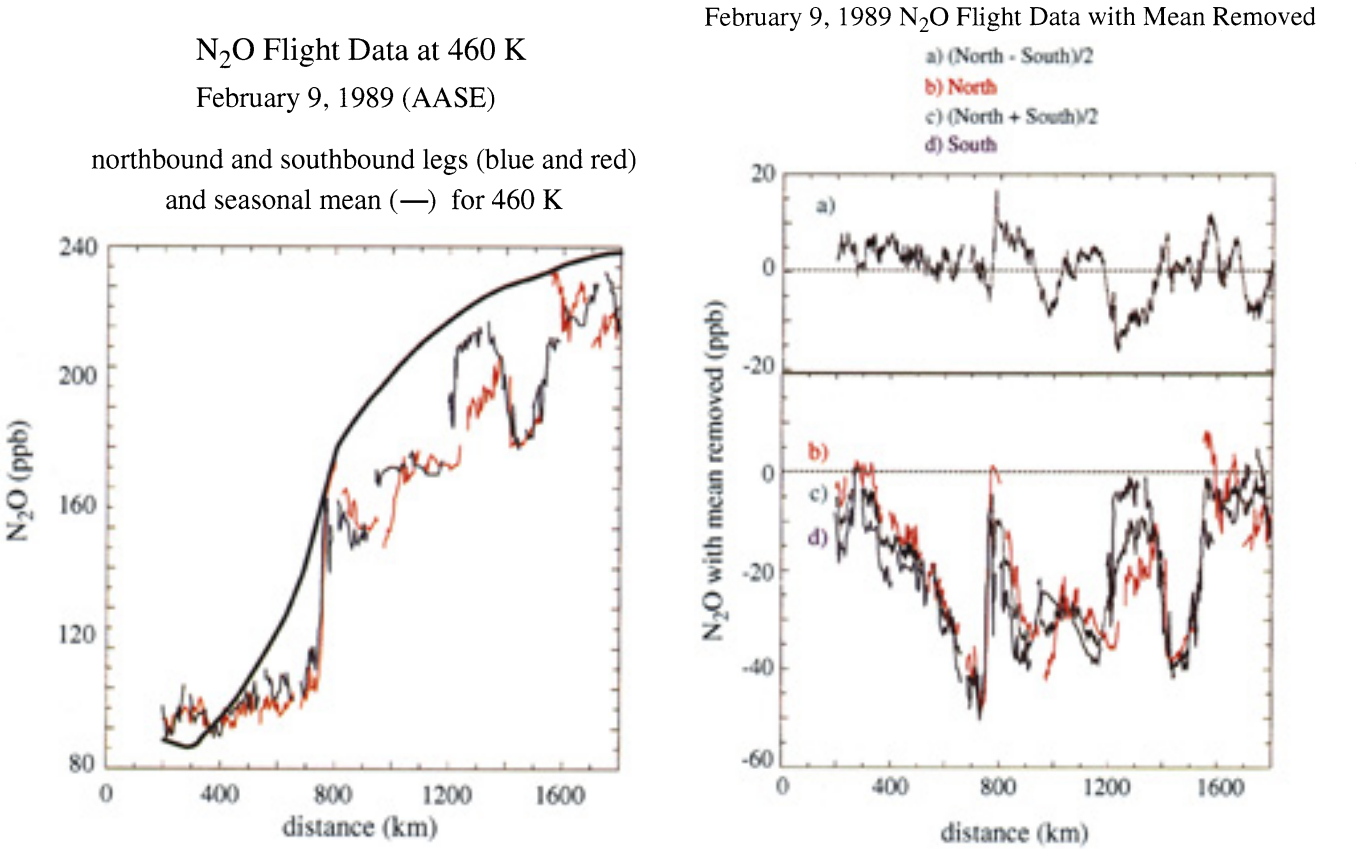

Plate 1. (a) N_2O from the northbound and southbound flight legs on February 9, 1989, measured on the 460 K surface. Also shown is mean N_2O for that isentropic surface and location with respect to the vortex (calculated from the mean of all AASE flights). (b) The bottom three traces are the flight data from Plate 1a with the mean removed and their average; the top trace is the difference of the two flight legs. The "sum" and "difference" time series show very different structures.

(Recall that the power spectrum is the square of the Fourier coefficients.) To put this another way, the total power spectrum, for example Figures 1 to 3, is composed of variability from different sources acting over different timescales, which can be coarsely separated into two categories. Long-lived atmospheric features (those showing little change over a few hours) are argued to produce the PWD spectrum, while processes causing variability on timescales of hours or less (e.g., small-scale mixing and gravity wave breaking) are assumed to produce the remainder of the power in the total spectrum. Note that the average of the spectra of the individual flight leg residuals is exactly equal to the "sum" spectrum plus the "difference" spectrum:

$$1/2\{ [FT(N_i')]^2 + [FT(S_i')]^2 \} = [FT(N_i' + S_i')]^2 + [FT(N_i' - S_i')]^2$$

or total power is equal to planetary wave debris power plus power from other sources. Details of this method of spectral "separation" are provided in the Appendix. Using this technique it is possible to diagnose some sources of tracer variability in the model and the observations and therefore attempt to assess whether SKYHI generates variability for the right physical reasons. This separation does not provide a unique separation of PWD from "other" sources. It is, however, the only separation allowed by the aircraft data. We assume the comparison between "fast" and "slow" relative to SKYHI model behavior is physically meaningful.

To perform this calculation, flight segments having nearly identical latitude, longitude, and potential temperature on both the northbound and the southbound flight legs are needed, but this requirement is met on only a subset of the flight days. Table 1 lists the AASE and AAOE flight days for which these conditions are met. For AASE, these flight segments range in length from 176 to 1600 km (mean = 712 km). For AAOE there are only five flights that can be used in this calculation, but their average length is ~1200 km, providing good scale overlap with SKYHI.

As mentioned before, the ER-2 cannot fly precisely on an isentropic surface but is generally within 5 K of one. The deviations are in part due to buoyancy motions of air parcels that the aircraft flies through. It is desirable to reduce the variance in the power spectrum that is associated with vertical displacement of parcels and aircraft motions. This has been achieved using the mean N_2O vertical gradient at each potential temperature/latitude coordinate in the flight leg, which is calculated from the mean fields given in part 1. Using the local vertical gradient, each data point of the flight segment is extrapolated to a fixed isentropic surface. This extrapolation, while only an approximation to the tracer mixing ratio on a true isentropic surface, is essential to produce a meaningful comparison between the observations and the model (where exact isentropic surfaces are used). For example, a flight leg with a potential temperature range of 460 ± 5 K would have each data point linearly extrapolated to its value on the 460 K surface using the mean N_2O vertical gradient at that point. The power spectrum calculated with the "quasi-isentropic" (unextrapolated) data has the same shape but with about 1.5 times the power of the "extrapolated data" spectrum, confirming that this procedure removes significant variance. As a final step in preparing the data, a split bell cosine taper was applied to the first and last 5% of the points of each flight segment to reduce end effects in the Fourier transform.

SKYHI - Simulated Flights

SKYHI is a three-dimensional general circulation model with 1° latitude by 1.2° longitude resolution and 40 vertical levels extending to 80 km. There are six pressure levels within the altitude range surveyed by AASE and AAOE (47 to 167 mbar). For further description of SKYHI see part 1 and references therein. "Flights" through the model output were simulated so that calculations performed on the observations could be duplicated using model output. Normally, SKYHI data are archived every 12 hours; to create a model "flight" that simulates the time dependence of the aircraft observations, the model was rerun so that hourly data could be saved. Because the 1° latitude SKYHI model is computationally expensive, only a limited number of flights were simulated.

Table 1. AASE and AAOE Flight Data Used in the Spectral Separation

No. of Flight Segments	Date	Potential Temperature, K	Length, km
		AASE	
9	January 7, 1989	490	821
	January 12, 1989	460	1090
	January 16, 1989	445	445
	January 16, 1989	445	238
	January 19, 1989	440	840
	January 20, 1989	440	176
	January 25, 1989	440	253
	January 30, 1989	430	946
	February 9, 1989	465	1600
		AAOE	
5	August 28, 1987	420	594
	August 30, 1987	425	1607
	September 2, 1987	430	1081
	September 4, 1987	425	1434
	September 20, 1987	460	1234

AASE, Airborne Arctic Stratospheric Experiment; AAOE, Airborne Antarctic Ozone Experiment.

For the Arctic, 12 days were selected that spanned model days December 25 to February 15; for the Antarctic, 10 days between August 16 and October 1 were selected. These particular time periods were chosen to cover the dates of the observation periods and include about a week before and after those dates. Model "flights" are 4-5 days apart.

Model "flights" cover a slightly larger latitude range than the real flights. This was desirable for two reasons: first, to make sure each flight included regions both outside and inside the polar vortex (see discussion on vortex location in part 1) and, second, to obtain FT information at wavelengths of several thousand kilometers, although this is not possible using the flight data. In each hemisphere, flight data were simulated for the same range of longitudes and isentropic surfaces as the observations.

SKYHI simulated flights are composed of hourly model output to parallel the time series nature of the actual flight data. The ER-2 covers as much as 23° latitude in 3.5-hour-long mostly meridional flight tracks. Using model results saved hourly, each flight leg was simulated by piecing together 6°-long segments (seven grid points) from consecutive model hours, four segments per flight leg. The seventh point of one hour was averaged with the first point of the next hour to smooth transitions. For example, a simulated flight out of Chile would begin (southbound) at 55°S (hour 1) and end at 81°S (hour 4), and the return leg (northbound) would begin at 81°S (hour 5) and end at 55°S (hour 8), for a total elapsed time of 7 hours.

The temporal composition of the simulated flight legs has a major impact on the results of the spectral separation. Experiments were performed using simulated flight legs that had no time dependence (i.e., all points of the simulated flight were from a single model time step), but with the elapsed time between the outbound and inbound legs varying from 1 to 11 hours. As the time lag increased, the fraction of total power coming from PWD decreased, and the smaller the scale, the more rapidly the PWD decreased with increasing time lag. This result is somewhat intuitive: the longer the lag between sampling, the more time small-scale mixing and advection have to deform and change the original features.

Results

Figures 4a, 4b, and 4c show the results for separation of the total power spectrum into the PWD and non-PWD (random phase) components for the Arctic (AWI and AWII) and the Antarctic, respectively. In each figure, the top line is the total power spectrum, the middle line is the PWD spectrum (for clarity, offset by one decade), and the bottom line is the remaining random phase power (offset by two decades). The 95% confidence intervals for each spectrum are also shown. Because the small sample size for AASE and AAOE results in noisy power spectra, the results shown are the fit of the spectra to a line. (The log of the total power and the random phase power are fit to a line. Using the fitted line parameters, the PWD power is calculated by subtracting the random phase from the total power.) The total power spectra in Figure 4 give the same information as Figures 2 and 3, but now new quantities are available (the PWD and non-PWD spectra) that reveal details of variability generated by processes occurring on different timescales. Slight differences between total power spectra in Figure 4 and Figures 2 and 3 result from differences in the number of days and the lengths of the flight segments that were used in the calculations.

SKYHI AWI shows the best agreement with data (Figure 4a): both the PWD and the non-PWD spectra are in excellent agreement with the slope and amplitude of the AASE calculation. The SKYHI 95% confidence intervals are very narrow and fall well within the AASE intervals shown. The results for the second Arctic winter shown in Figure 4b show that despite the enormous improvements in N_2O morphology in and around the polar vortex in AWII (part 1), the AWII spectral separation results do not agree as well with the observations as AWI does. Although the model PWD and total power spectra are mostly within the AASE confidence intervals, the non-PWD component is too large by a factor of

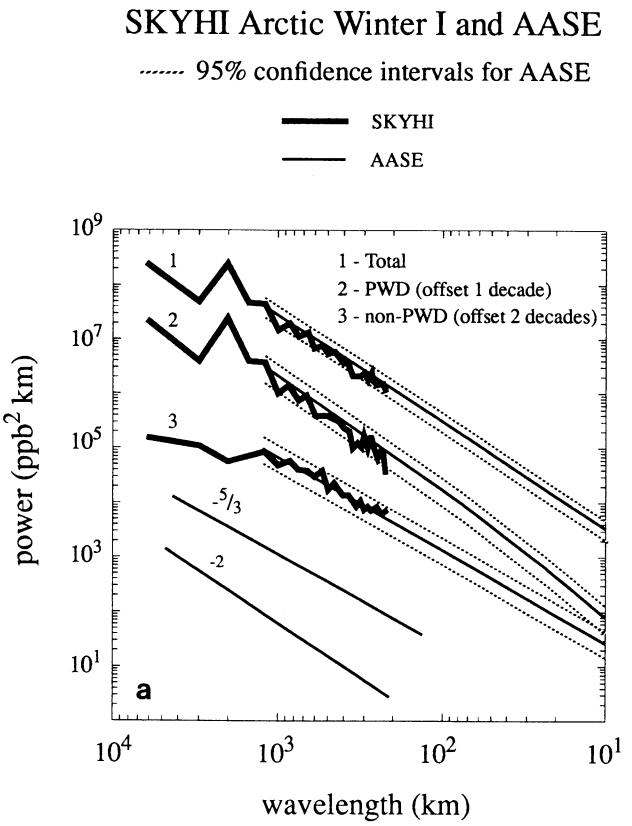

Figure 4. Comparison of spectral separation results for AASE, AAOE, and SKYHI. In each figure the dashed lines represent the 95% confidence intervals for the measurements. Because the SKYHI confidence intervals are so much narrower than the AASE or AAOE intervals, they are not shown. For all figures, SKYHI 95% confidence intervals are ±13% for total power and ±18% for the other two spectra. The top spectrum is the total power. The planetary wave debris (PWD) spectrum is second and is offset by one decade for clarity. The non-PWD spectrum is third and is offset by two decades. (a) AASE (nine flights) and SKYHI Arctic winter I (AWI). SKYHI shows PWD power and non-PWD (random or "noise" power) in close agreement with that calculated from the observations. The AASE slopes in the region of overlap with SKYHI are (1) -1.9, (2) -2.0, and (3) -1.7. (b) AASE (nine flights) and SKYHI AWII. SKYHI shows total and PWD power in close agreement with that calculated from the observations, but the model has greater short timescale variability. (c) AAOE (five flights) and SKYHI Antarctic winter. The AAOE slopes in the region of overlap with SKYHI are (1) -1.8, (2) -2.1, and (3) -1.7.

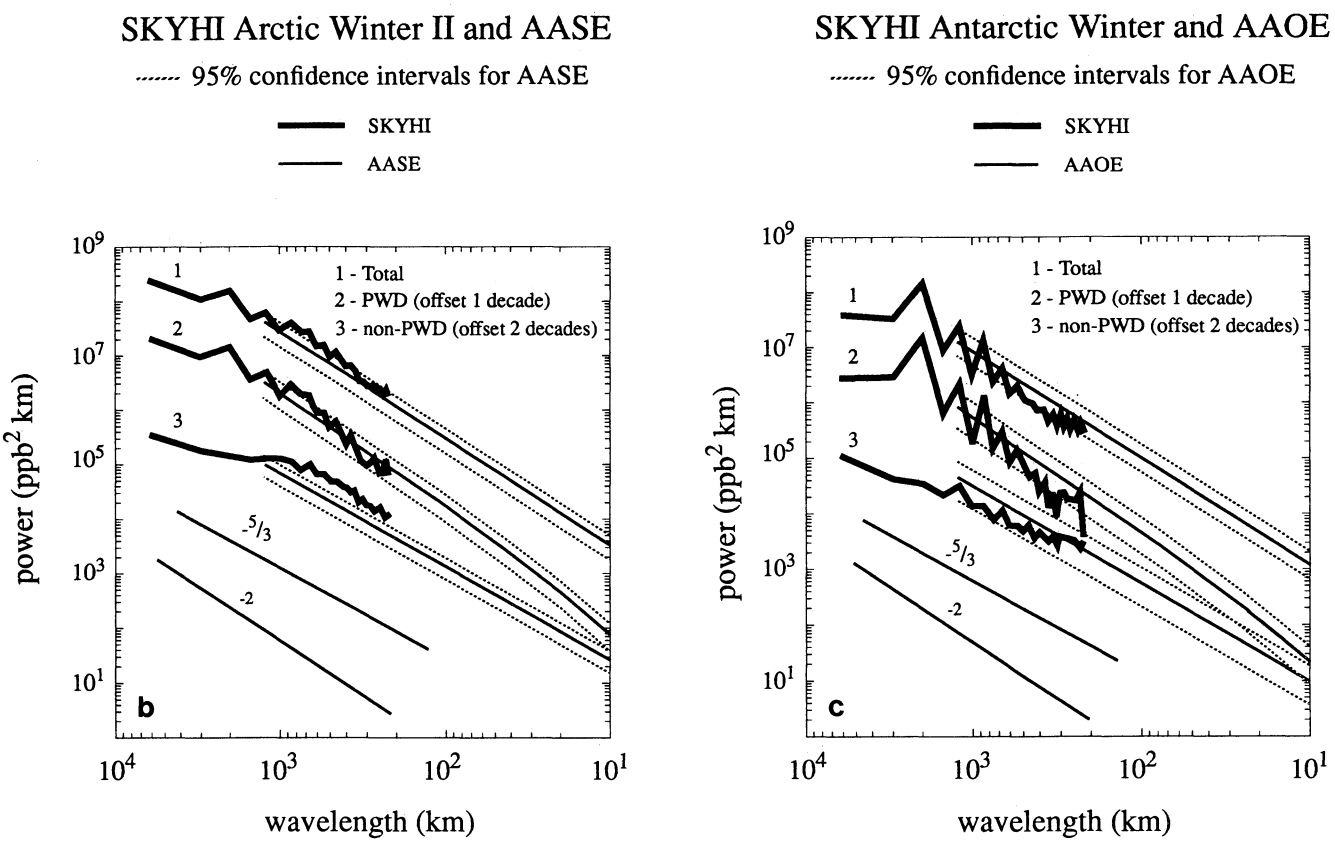

Fig. 4. (continued)

2-3. It is difficult to say whether this represents a true excess of short timescale variability, or simply that SKYHI AWII is a more active winter than 1989, resulting in a poor synoptic match.

Although Figure 3 shows excellent agreement between AAOE and Antarctic SKYHI spectral slopes, Figure 4c suggests that this may be fortuitous and not an indication of similarities in the underlying physical forcings that determine the spectral slope. In Figure 4c, although all the model spectra fall within the 95% confidence intervals of the AAOE spectra, the model PWD power drops off rapidly below ~700 km (to roughly a -3 slope) resulting in somewhat inadequate PWD power below ~500 km, and the random phase power is close to becoming a noise spectrum (slope 0) below 400 km. It appears that noise in the model represents a significant contribution to the power spectrum at this scale. A flattened slope is also visible in the total power spectrum below 300 km.

Model flights on isobaric surfaces can also be simulated using the method previously described, and the diagnostic methods used above can be applied to separate PWD and non-PWD power on isobaric surfaces. This calculation was performed as a check of the robustness of the separation analysis, that is, to see if the same calculation done on isobaric surfaces would give approximately the same results. Because the thickness of planetary wave disturbances is large compared to the difference between isobaric and isentropic surfaces over scales of hundreds of kilometers, a priori we expect the PWD spectrum in both calculations to be approximately the same. The differences one might expect between the two analyses would be the power from adiabatic motions, primarily buoyancy or gravity waves (contributors to the non-PWD power in the case of isobaric spectra). Because gravity wave oscillations are essentially adiabatic motions, they cause little change in the potential temperature of an air parcel, and vertical displacements resulting from gravity wave motion will be nearly "invisible" on an isentropic surface. Pressure surfaces chosen for this calculation cover the same altitude range as in the isentropic analysis, and the same model days and longitudes are used. For both hemispheres the PWD spectra for the isentropic and the isobaric analyses are nearly identical, but as expected, the non-PWD power for the isobaric analysis is greater. This agreement in the PWD power gives us additional confidence in the robustness of planetary wave debris as a measurable and meaningful quantity.

3. Interpretation of the Spectral Separation

The purpose of this calculation is twofold: to understand the relevant scales over which different processes create variability in the real atmosphere and then from that standpoint to assess whether SKYHI is producing tracer variability in the same way as the real atmosphere. Expressing the PWD power as a percentage of total power reveals the scales over which variability caused by planetary wave breaking debris is significant. The statistical significance is limited in each case by the number of flights available for this calculation and by the inexact nature of this analysis (i.e., the return flight leg will not sample the same air observed on the outbound leg due to advection).

Figure 5 compares PWD percentage of the total power for AASE and AAOE, derived from the linear fit of the spectra

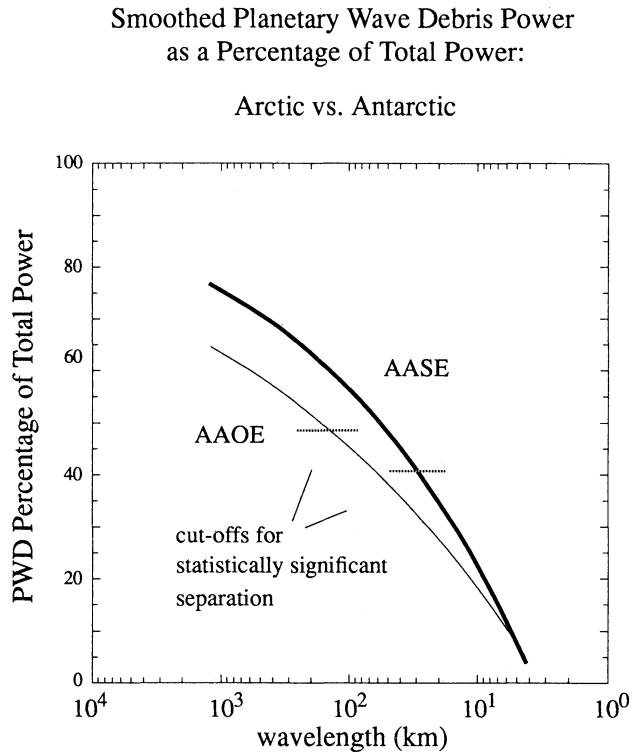

Figure 5. Comparison of AASE and AAOE PWD power as a percentage of total power. The curves shown are derived from the fitted spectral results shown in Figure 4. The small number of flights available for these calculations puts a lower limit on the scale at which the separation is statistically significant, about 140 km for AAOE and ~30 km for AASE.

shown in Figure 4. What this figure shows is that in spite of the small sample size, atmospheric variability from PWD is a statistically significant contributor to total variability in the real atmosphere, at least down to 140 km in the Antarctic and down to 30 km in the Arctic. Because both these numbers are of the same order as the model grid spacing, it is possible to comment on how successful the model is at generating variability at the right scales for the right reasons. In Figure 4a the SKYHI AWI separation shows excellent agreement with the AASE results at all scales of overlap. From this we conclude that as far as can be determined from this analysis, the processes that generate both the slowly varying and the more rapidly varying tracer features in the model are sufficient, and each is creating appropriate variability at scales from 220 to 1200 km. In Figure 4b, only at 1200 km do all SKYHI AWII spectra agree well with AASE. The SKYHI PWD spectrum is in good agreement with AASE at all scales, suggesting that planetary wave breaking and the associated ripping and shredding of material from the vortex edge is occurring to an appropriate degree in the lower stratosphere. The SKYHI non-PWD spectrum reveals an excess of short timescale variability, or "noisiness" at scales below 1000 km. This could result from the variability being produced at too great a rate (e.g., too much gravity wave breaking), from variability being damped too slowly (insufficient subgrid scale diffusion), or from differences in the level of wave activity in AWII and the 1989 winter (akin to the interannual variability one expects in northern hemisphere winters).

SKYHI Antarctic results are more difficult to assess due to the small AAOE sample size. Because of the wide confidence intervals for the AAOE spectra, there is no clear-cut disagreement with the SKYHI spectra. However, at scales below 500 km the SKYHI total and PWD spectra border on being lower than AAOE in a statistically meaningful way and the slopes of all three SKYHI spectra are different than the AAOE slopes. (Recall that Figure 3, calculated with a larger data set, strongly suggests inadequate total power in the model Antarctic.) The PWD power has a -3 slope between 400 and 700 km, suggesting that there is either a lack of wave breaking activity in the model or that diffusion is dissipating the variance too rapidly. And although the model non-PWD spectrum is in rough agreement with AAOE, below 500 km the relatively flat slope suggests some of the short timescale variability may come from model (numerical) noise. A flat spectrum below 300 km is also discernible in the total power spectrum. A diagnosis of insufficient wave activity in the model Antarctic winter would be consistent with the too low 50-mbar temperatures near the pole discussed in part 1. The SKYHI Antarctic lower stratosphere appears to produce total variability that is not too different from AAOE but gets that variability more from short timescale fluctuations rather than from slowly varying features that can be generated by planetary wave breaking activity.

Figure 6 compares all PWD and non-PWD results for both hemispheres. Planetary wave debris power is greater in the northern hemisphere winter for both the model and the observations, by a factor of ~3 between AASE and AAOE, and a factor of 2-5 for the model. The upper panel clearly shows missing PWD below 600 km in the SKYHI Antarctic. Non-PWD power is also greater in the Arctic than in the Antarctic for both the model and the observations, by a factor of 2 for the observations but by up to a factor of 10 for the model. The bottom panel reveals a lack of short timescale variability in the SKYHI Antarctic but an excess of it in the second SKYHI Arctic winter. Overall, SKYHI is more successful at simulating the more dynamically active hemisphere.

Hemispheric differences in the PWD spectra may be accounted for by large hemispheric differences in high-latitude topography and tropospheric circulation: above 50°N there is much mountainous terrain, while 50°-70°S is almost entirely ocean and the only land mass (Antarctica) is in a nearly zonally symmetric position over the pole. Radar and balloon studies have reported turbulent layers in the northern winter lower stratosphere that appear to be due to breaking gravity waves which may be topographically forced [*Barat*, 1982; *Sato and Woodman*, 1982]. Hemispheric differences are seen in the comparison of geopotential height amplitudes for wavenumbers 1 and 2 in January and July, where high-latitude northern winter wave amplitudes are a factor of 2-4 greater than their southern counterparts [*World Meteorological Organization* (WMO), 1986]. While SKYHI correctly produces a northern hemisphere stratosphere that is more dynamically active than the south, the model's weak dynamical forcing in the south causes an exaggeration of the differences.

These spectral results lead to some puzzling questions. The dominance of the PWD in the total spectrum in both the data and the model casts doubt about traditional gravity wave arguments invoking either saturation or energy reverse cascade processes in interpreting observed mesoscale spectral slopes,

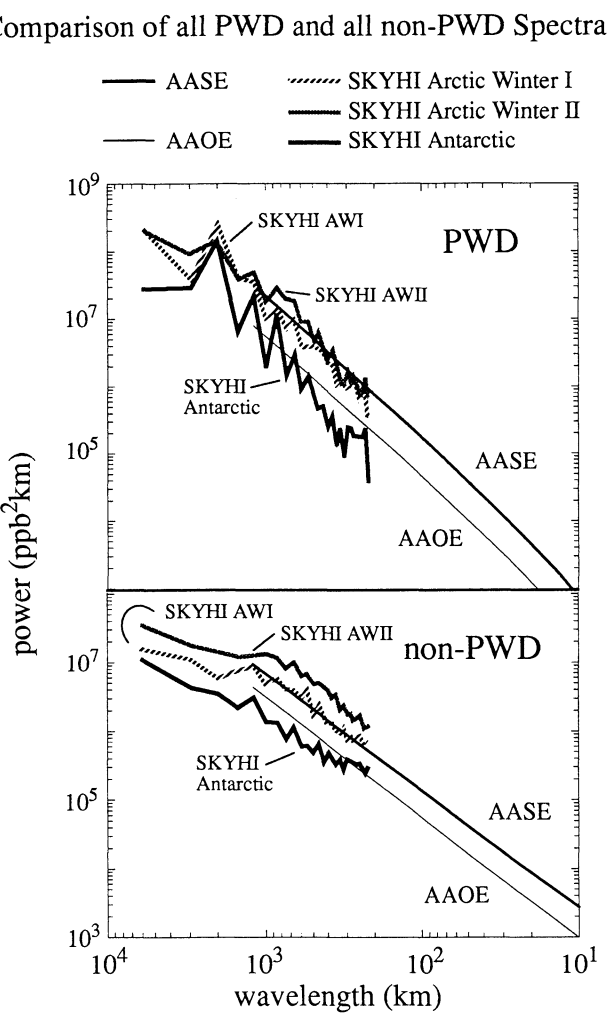

Figure 6. (Top) Comparison of all PWD power calculated: AASE, AAOE, and SKYHI (AWI, AWII, and Antarctic). All Arctic spectra show greater power than the Antarctic spectra. (Bottom) Comparison of all non-PWD power calculated. Again, the Arctic shows greater power here. Non-PWD power for AWII is much greater than AWI; see text for discussion.

at least in the polar lower stratosphere. The aircraft data suggest a quasi-two-dimensional variance cascade in the isentropic plane. If a simple two-dimensional cascade were operative, however, the expected N_2O variance should be close to a -1 slope. SKYHI, AAOE, and AASE spectra are decidedly steeper than that, around -5/3 to -2.

This leaves us well short of a phenomenologically sound explanation of the observed -5/3 to -2 slopes. A speculation is that the cascade is indeed quasi-two-dimensional but that radiative damping, shear-induced instability, and gravity wave breaking at smaller scales produce more variance dissipation at 10- to 1000-km scales than implied in a classical two-dimensional cascade regime. We regard this issue to be unresolved but one that provides an intriguing challenge for future theoretical and modeling research.

Discussion of the Diabatic Circulation in SKYHI

The Arctic. Wave activity not only generates tracer variability but also drives the diabatic circulation. By combining the spectral separation results with the temperature and tracer field comparisons presented in part 1, some aspects of the diabatic meridional circulation in SKYHI may be evaluated. Analysis of the Arctic PWD power indicates that SKYHI is able to generate realistic amounts of wave-breaking activity in the Arctic winter lower stratosphere. The agreement of spectral slopes suggests that SKYHI's parameterized diffusion is reasonably chosen, damping the cascaded variance to smaller scales at roughly the right rate. Because wave activity forces the dynamical heating that drives the pole from radiative equilibrium, agreement of model temperatures with observations is also an indication of sufficient wave forcing. In part 1 both model Arctic winters were shown to have 100-mbar temperatures inside and outside the vortex that are in excellent agreement with the 1989 observed temperatures, while 50-mbar temperatures are slightly lower than observed (3-4 K) inside the vortex. Because these 1989 temperatures were unusually low, this comparison is more favorable to SKYHI than would a more "typical" January and thus some weakness may remain in the model wave forcing. A small inadequacy might not be seen in the spectral separation results because of the fairly wide 95% confidence intervals of the AASE results. The temperature comparison, the mean N_2O structure, and the spectral results all support the conclusion that SKYHI has a realistic diabatic circulation in the Arctic.

Although these results are not necessarily typical of the SKYHI climatological mean, an unknown, it should be noted that the two SKYHI Arctic winters were different (one much warmer than the other), yet both have a favorable comparison with the AASE results. A 10-year climatology of the 3° latitude resolution SKYHI shows Arctic winter lower stratospheric temperatures very similar to AWI and AWII temperatures, providing some assurance that the 1° SKYHI results are probably not due to anomalously and hence fortuitously warm model winters.

Comparison of mean N_2O fields provides additional insight into the competing processes that determine the stratosphere's N_2O structure. Diabatic descent inside the vortex moves the N_2O isopleths downward near the pole, while wave breaking in the "surf zone" outside the vortex produces strong mixing, bringing midlatitude air (with higher N_2O mixing ratios) toward the edge. Both of these processes sharpen the N_2O gradient at the edge. Parameterized diffusion and advective transport across the edge lessen the gradient. Recent calculations by *Schoeberl et al.* [1992] have quantified these edge sharpening effects by using the AASE data to calculate N_2O flux and eddy flux convergence. They showed that the region of maximum flux was located on the anticyclonic side of the jet, where relatively high N_2O mixing ratios were being "diffusively transported" toward the pole. Just inside the vortex the diffusive flux dropped to zero, while farther inside, it was negative, a result of the descent of higher-altitude air having lower N_2O mixing ratios. The balance of these processes generates the observed mean gradient at the edge. The remarkable similarity between N_2O gradients at the vortex edge in AWII and AASE suggests that SKYHI has achieved the right balance between these processes.

The Antarctic. The inadequate model wave activity shown in Figure 4c produces a weakly forced southern hemispheric circulation, and the low 50-mbar temperatures inside the vortex are likely a direct result of this. The SKYHI Antarctic mean N_2O field, shown in Figure 8b of part 1, provides further evidence for a weak model diabatic circulation. The low polar temperatures in the model Antarctic result in small radiative

cooling rates, leading to insufficient descent and model N_2O mixing ratios that are too high. Outside the vortex, SKYHI mean N_2O gradients on isentropic surfaces are very similar to AAOE gradients, while inside the vortex, AAOE gradients are substantially steeper. But compared to the Arctic, the AAOE tracer gradients are relatively flat and imply that the southern circulation is comparatively weak. Calculations by *Schoeberl et al.* [1992] show that N_2O flux convergences at the edge and inside the Antarctic vortex are extremely small even at 400 K, indicating that this is a region of very weak mixing.

The relatively flat SKYHI edge gradients indicate that the model has inadequate mixing in the southern hemisphere "surf zone." Because strong wave forcing generates the "surf zone" and sharpens the edge gradient, the relatively flat edge gradients, combined with the inadequate PWD spectrum and low vortex temperatures, support the conclusion that SKYHI's wave-forced diabatic circulation is too weak in the southern hemisphere. As a result, the diffusion, which may be appropriate in a stronger dynamical regime, appears too strong in this weak wave-forcing case. The too steep PWD slope below scales of 700 km also supports the idea that there is inadequate PWD power available to balance the rate of diffusion (resulting in slope steepening).

Judging by the time needed to establish tracer equilibrium in the SKYHI Arctic, the second SKYHI Antarctic winter will probably have much lower tracer mixing ratios than the first winter. N_2O isopleths in the second SKYHI June have moved down considerably compared to the first June, and as discussed in part 1, it is estimated that the lower tracer isopleths of the second June will lead to more realistic mixing ratios in the second August and September and to steeper edge gradients.

4. Global Circulation in SKYHI

Comparison with the GFDL General Circulation/ Tracer Model

In section 3.2 (Comparison with observations) of *Mahlman et al.* [1986] (hereafter referred to as MLM86), vertical profiles of balloon observations of N_2O at three latitudes (equatorial, midlatitude, and polar) reported by *Goldan et al.* [1980] were compared to output from the GFDL general circulation/tracer model using three different destruction rates (fast, regular, and slow). The prescribed "regular" N_2O destruction chemistry used in this model is the same as in 1° and 3° latitude versions of SKYHI and is described in part 1. The "fast" chemistry profiles agreed with the observations at middle and high latitudes, and the "slow" chemistry gave good results at the equator, but none of the destruction rates agreed well with observations at all three latitudes. Since variations in the destruction rate alone could not give suitable agreement everywhere, they reasoned that the diabatic meridional circulation was important in controlling tracer profiles. They also noted that model mean meridional tracer isopleths were not as steep as the real ones by ~30%, i.e., there was too little equator-to-pole gradient.

The results presented in MLM86 clearly illustrate weak meridional circulation in the general circulation/tracer model. Slow chemistry looked the best at the equator because the effect of a slow destruction rate is equivalent to that of increased rising motions in the tropics. Fast chemistry looked best at middle and high latitudes where its effect was equivalent to that of stronger descent (bringing down lower mixing ratios from above). Figure 7 compares the "regular" chemistry in MLM86 with the same balloon data and the 1° SKYHI profiles using the same "regular" chemistry. The SKYHI profiles are overall in better agreement with the balloon data than are the GFDL tracer model results, especially at the equator. Comparing the results at the equator and Antarctica clearly shows SKYHI's steeper equator-to-pole gradient. The SKYHI profile is in excellent agreement with the balloon data near the equator but has slightly high mixing ratios at middle and high latitudes below 30 mbar. The comparison at middle and high latitudes could be improved by increasing the chemical destruction rate, or by increasing downward transport in the stratosphere. The effect of faster chemistry is to flatten meridional slopes but only where the photochemical lifetime of N_2O is shorter than about 700 days (MLM86). Thus in the lower stratosphere where the photochemical lifetime of N_2O is much longer than that, the effect of a slight increase in the destruction chemistry might be to bring better agreement at middle and high latitudes with only a small effect on the good agreement in the tropics. More likely, an improvement in the agreement could be achieved by an increase in model wave activity to strengthen the southern diabatic circulation, which will increase poleward, downward transport. The latter possibility is supported by spectral results presented in the previous section and by the mean N_2O fields shown in part 1.

Some Comments About SKYHI

Mahlman and Umscheid [1987] have shown that increasing the horizontal resolution of SKYHI from 9° to 5° to 3° to 1° latitude resolution has stepwise improved (raised) winter polar stratospheric temperatures from the 0.3- to 50-mbar levels. Increasing horizontal resolution produces major improvements in temperatures, winds, and transport in the SKYHI stratosphere and mesosphere by extending the allowable frequency range of planetary and gravity waves. Some of the effects of this improvement can readily be seen in the tracer vertical profiles in Figure 7, where SKYHI 1° is compared to the GFDL tracer model that has coarser resolution (2.4° latitude) and a top level at 10 mbar. Here and in part 1, SKYHI model results from both winter poles have been compared to observations, and it was shown that problems still exist in the temperatures and tracer fields in the lower stratosphere, primarily in the Antarctic. Breaking gravity waves in the stratosphere having scales of less than 110 km may be important in the vertical momentum flux convergence in the southern hemisphere, and their inclusion might lead to deceleration of the excessively high zonal winds and concomitant heating in the Antarctic stratosphere. Agreement with observations in the lower stratosphere may not come about until model horizontal resolution reaches 0.25° or 0.5°. Vertical resolution, relatively coarse at present (~1.7 km), is likely to require a substantial increase.

In spite of the encouraging results presented here, SKYHI remains a limited representation of processes occurring in the atmosphere. Although high horizontal resolution is essential for producing good comparisons with observations, is higher resolution the only requirement for further improvements in transport and dynamics? Because of the large impact of radiative effects on atmospheric dynamics, advances in model performance may also come from improvements in the prescribed O_3, from the addition of the effects of the greenhouse gases CH_4, N_2O, CFC-11, and CFC-12, and from

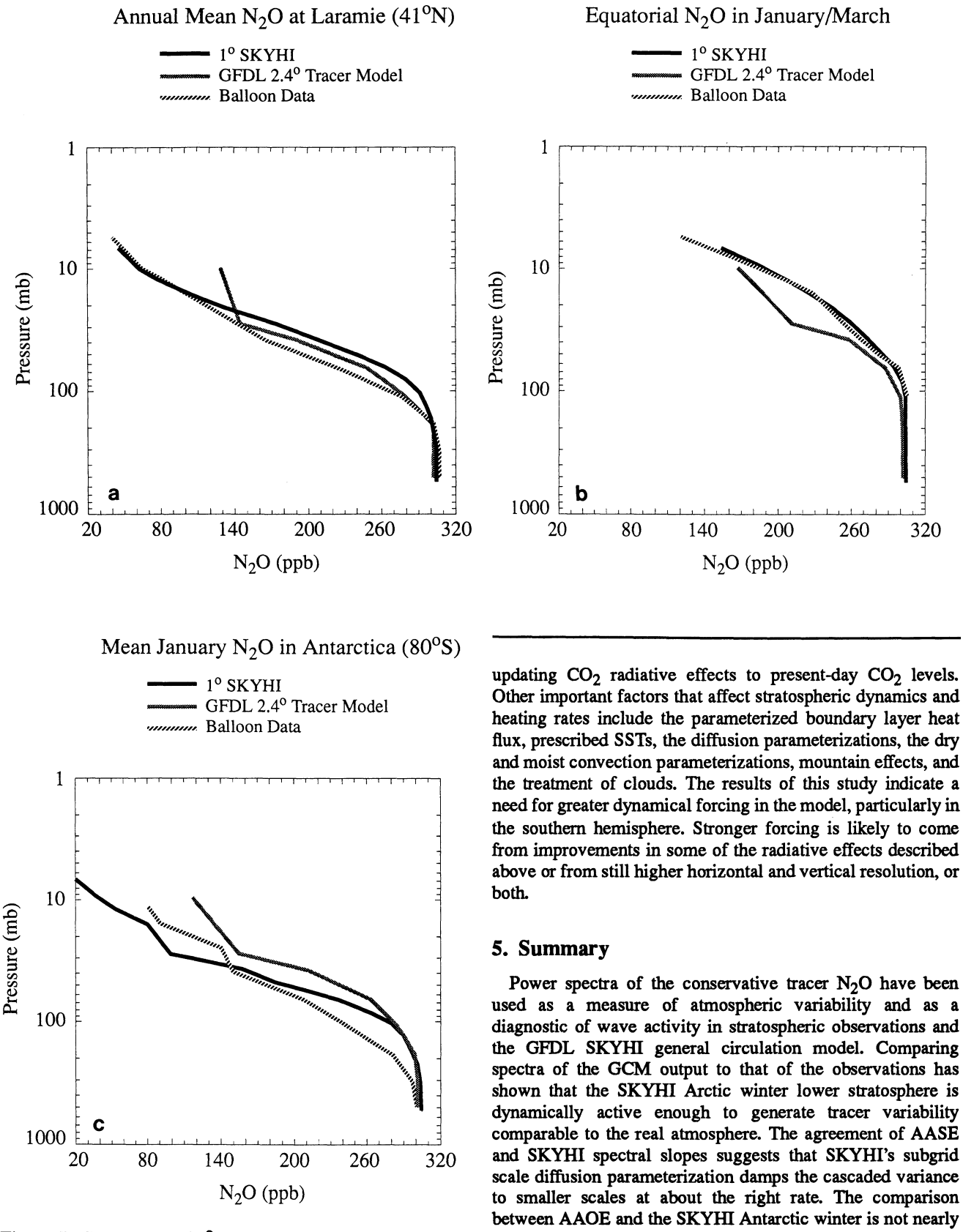

Figure 7. Comparison of 1° latitude resolution SKYHI results (solid curve), 2.4° GFDL tracer model N_2O vertical profiles from MLM86 (shaded), and balloon measurements [*Goldan et al.*, 1980] (dashed). (a) Annual mean at Laramie, Wyoming (41°N). (b) January/March mean at Canal Zone (9°N and 5°S). (c) January mean at Antarctica (80°S).

updating CO_2 radiative effects to present-day CO_2 levels. Other important factors that affect stratospheric dynamics and heating rates include the parameterized boundary layer heat flux, prescribed SSTs, the diffusion parameterizations, the dry and moist convection parameterizations, mountain effects, and the treatment of clouds. The results of this study indicate a need for greater dynamical forcing in the model, particularly in the southern hemisphere. Stronger forcing is likely to come from improvements in some of the radiative effects described above or from still higher horizontal and vertical resolution, or both.

5. Summary

Power spectra of the conservative tracer N_2O have been used as a measure of atmospheric variability and as a diagnostic of wave activity in stratospheric observations and the GFDL SKYHI general circulation model. Comparing spectra of the GCM output to that of the observations has shown that the SKYHI Arctic winter lower stratosphere is dynamically active enough to generate tracer variability comparable to the real atmosphere. The agreement of AASE and SKYHI spectral slopes suggests that SKYHI's subgrid scale diffusion parameterization damps the cascaded variance to smaller scales at about the right rate. The comparison between AAOE and the SKYHI Antarctic winter is not nearly as favorable. Although there is good agreement of the spectral slopes, SKYHI shows inadequate power at scales of 220-3000 km, indicating too little variability in the model Antarctic stratosphere.

Spectral analysis has been applied to aircraft N_2O observations in an attempt to discriminate between different

sources of variability. All sources of variability contribute to the tracer power spectrum. Atmospheric features that are long-lived (i.e., that can be observed with little change over a period of many hours) are argued to be the debris from planetary wave breaking, while processes that cause variability on timescales of a few hours (e.g., gravity wave breaking, mixing, and advection) are assumed to produce the remainder of the observed variability. Using the spectral separation technique described, some sources of tracer variability in SKYHI and the observations have been diagnosed. Because the diabatic meridional circulation is driven by wave activity, the results of the spectral separation are also useful in evaluating the model diabatic circulation. "Flights" through the model data were simulated so that calculations performed on the observations could be duplicated using model output.

Spectral separation results for both SKYHI Arctic winters compared favorably with the AASE data. The planetary wave debris spectra of AWI and AWII are in excellent agreement with the slope and amplitude of the AASE spectrum. Short timescale variability (the non-PWD spectrum) in AWI compares well with AASE, while AWII shows additional variability. In Antarctic SKYHI, although the total power spectrum has a -5/3 to -2 slope in agreement with AAOE, the separation shows that the agreement may be fortuitous. Although all the model separation spectra fall largely within the 95% confidence intervals of the AAOE spectra, the model PWD spectrum steepens below ~700 km, suggesting inadequate PWD power at these scales. Because the non-PWD power flattens to a slope between 0 and -1 below ~500 km, numerical noise in the model thus may represent a significant contribution to the power spectrum between 220 and 500 km.

Analysis of the SKYHI Arctic PWD power spectra indicates that the model is able to generate realistic amounts of wave activity in the Arctic winter lower stratosphere. Because wave activity drives the dynamical heating which pushes polar temperatures away from radiative equilibrium, agreement of model temperatures with observations provides evidence for adequate wave activity. Comparison of tracer fields provides additional insight into the polar stratospheric circulation. Wave-driven diabatic descent inside the vortex brings low N_2O air down, while strong quasi-horizontal mixing in the "surf zone" keeps mixing ratios high outside the vortex; together the processes create a sharp N_2O gradient at the vortex edge. The remarkable similarity between N_2O gradients at the vortex edge in AWII and AASE suggests that SKYHI has a sufficiently strong diabatic meridional circulation and wave activity in the northern hemisphere.

Weak wave activity near the SKYHI Antarctic vortex, suggested by the steep PWD spectrum below 700 km, leads to a weakened diabatic circulation and is likely the cause of the low 50-mbar temperatures (part 1). The SKYHI Antarctic N_2O field, shown in Plate 2b of part 1, provides further evidence for weak model diabatic circulation. Weak dynamical forcing leads to low polar temperatures and insufficient radiative cooling rates, and thus insufficient polar descent and high N_2O mixing ratios. SKYHI vortex edge gradients are less steep than the observations, indicating the model has insufficient mixing in the southern hemisphere "surf zone". Because wave forcing sharpens the edge gradient, the relatively flat edge gradients, inadequate PWD spectrum, and low vortex temperatures support the conclusion that the wave-forced diabatic circulation is too weak. The steepness of the PWD slope supports the idea that there is inadequate PWD power available to balance the rate of diffusion, resulting in slope steepening.

Overall, SKYHI is more successful at simulating the more dynamically active northern hemisphere. For the observations, at all scales, the Arctic (AASE) PWD spectrum has 2-3 times as much power as the Antarctic (AAOE) spectrum. Hemispheric differences in the PWD spectra may be accounted for by large hemispheric differences in high-latitude topography and tropospheric circulation. Because of inadequacies in the dynamics of the model southern hemisphere, the hemispheric difference in wave activity is exaggerated in SKYHI.

Both Antarctic and Arctic aircraft data show mesoscale spectral slopes of N_2O variance in the -5/3 and -2 range and similarly so for the SKYHI model. Moreover, both data and model indicate that most of the spectral power in the mesoscale subrange is due to "debris" from planetary wave breaking events. Yet, a purely two-dimensional isentropic variance cascade should produce close to a -1 spectral slope. These results suggest that the atmosphere's tendency for a two-dimensional cascade may be interrupted by enhanced dissipative processes that are activated by the cascade itself. This issue invites more focused theoretical and observational attention. It is encouraging that SKYHI reproduces this behavior reasonably well, but it may or may not be for the right reasons.

A more global evaluation of 1° SKYHI dynamics was made by a comparison with vertical profiles of balloon observations of N_2O at low, middle, and high latitudes and with output from the GFDL general circulation/tracer model [*Mahlman et al.*, 1986]. The 1° SKYHI profiles are overall in better agreement with the balloon data than are the GFDL tracer model results. Comparing the results at the equator and Antarctica clearly shows SKYHI's improved equator-to-pole gradient.

All model/observation comparisons in this paper and in part 1 point to one primary conclusion: SKYHI's dynamical forcing of the stratosphere is nearly sufficient in the northern hemisphere but lacking in the southern hemisphere. To steepen the southern hemisphere slopes requires a stronger diabatic meridional circulation. Improvement in the circulation may come about by improvement in the treatment of various radiative effects and by higher model resolution, where gravity waves having scales of less than 110 km will be able to increase the amount of wave activity flux convergence in the Antarctic lower stratosphere, resulting in higher polar temperatures and the deceleration of the excessively high zonal winds.

Appendix: Separation of Planetary Wave Debris (PWD) and Non-PWD Contributions Using Fourier Transform (FT) Analysis

The aircraft tracer data used in this paper are collected as a time series on an isentropic surface, with each flight consisting of an outbound and a return flight leg of up to 2200 km each. Assume there are two basic components to tracer variability observed during flight: one is a slowly varying component that is essentially unchanged over a 7-hour period (the maximum flight length) while the other is a more rapidly varying component, causing variability on a timescale of a few hours. The variability from each component can be defined as

(1) A ≡ the slowly varying component (planetary wave debris power), essentially identical on the outbound and return legs; (2) C ≡ the rapidly varying component (non-PWD power) of the outbound flight leg, equivalent to a random time series; (3) D ≡ the rapidly varying component (non-PWD power) of the return flight leg, also equivalent to a random time series, uncorrelated with C. Each flight leg can be thought of as being composed of two superimposed time series. The outbound (N, north) and return (S, south) time series can be defined as

$$N \equiv A + C$$
$$S \equiv A + D$$

and their Fourier transforms are

$$FT(N) = FT(A+C)$$
$$FT(S) = FT(A+D)$$

(For simplicity, time series such as N and S will not be subscripted to denote their length (e.g., N_i) as was done in section 2. Here, subscripting is used to denote different flight pairs.)

For two random time series C and D in the limit of a large number of pairs random time series, L, the sum of the transforms of the average of each random time series pair $((C+D)/2)$ is equal to the sum of the transforms of the difference of each pair $((C-D)/2)$. That is,

$$\sum_{i=1}^{L} FT\left((C_i + D_i)/2\right) = \sum_{i=1}^{L} FT\left((C_i - D_i)/2\right) \qquad (1)$$

Each flight leg is assumed to be composed of a coherent component (A) and an incoherent component (C or D). In the limit of a large number of flight leg pairs, the average of the power spectra of the flight legs (e.g., FT(N)) is equal the average of the spectra of the coherent components plus the average of the spectra of the incoherent components:

$$\{\sum_{i=1}^{L} [FT(A_i + C_i)]^2\}/L =$$
$$\{\sum_{i=1}^{L} [FT(A_i)]^2 + \sum_{i=1}^{L} [FT(C_i)]^2\}/L \qquad (2)$$

(The power spectrum is the square of the FT coefficients.)

This equation states that the power spectrum of a flight leg is equal to the power spectrum of the slowly varying component plus the spectrum of the rapidly varying component. Empirically, it can be shown that the average total power spectrum for a flight leg pair, $([FT(N)]^2 + [FT(S)]^2)/2$, is equal to the "sum" spectrum $([FT((N+S)/2)]^2)$ plus the "difference" spectrum $([FT((N-S)/2)]^2)$. For L northbound and L southbound legs,

$$\{\sum_{i=1}^{L} [FT(N_i)]^2 + \sum_{i=1}^{L} [FT(S_i)]^2\}/2L = \text{average total power}$$

$$\{\sum_{i=1}^{L} [FT(N_i)]^2 + \sum_{i=1}^{L} [FT(S_i)]^2\}/2L =$$

$$\{\sum_{i=1}^{L} [FT((N_i + S_i)/2)]^2 + \sum_{i=1}^{L} [FT((N_i - S_i)/2)]^2\}/L$$

Dropping the summations and the "/Ls," and substituting with the definitions of N and S, this can be rewritten

$$1/2\ \{[FT(A+C)^2 + [FT(A+D)^2\} =$$
$$[FT((A+C) + (A+D))/2]^2 + [FT((A+C) - (A+D))/2]^2$$

$$1/2\ \{[FT(A+C)^2 + [FT(A+D)^2\} =$$
$$[FT(A+(C+D)/2)]^2 + [FT((C-D)/2)]^2$$

Using relationship (2), this can be rewritten as

$$1/2\ \{[FT(A+C)^2 + [FT(A+D)^2\} =$$
$$[FT(A)]^2 + [FT((C+D)/2)]^2 + [FT((C-D)/2)]^2$$

And using relationship (1), this is equivalent to

$$1/2\ \{[FT(A+C)^2 + [FT(A+D)^2\} = [FT(A)]^2 + 2[FT((C-D)/2)]^2 \qquad (3)$$

or average total power is equal to coherent (PWD component) plus incoherent (non-PWD component).

Note that $[FT((N-S)/2)]^2$, the "difference" spectrum, is identical to $[FT((C-D)/2)]^2$. The spectrum of just the slowly varying, planetary wave breaking debris component is obtained by rearranging (3)

$$[FT(A)]^2 = 1/2\ \{[FT(N)]^2 + [FT(S)]^2\} - 2[FT((N-S)/2)]^2$$

In practical terms the pure PWD component of the average total power spectrum is obtained by subtracting 2 multiplied by the difference spectrum from the total power spectrum.

Acknowledgments. The authors express thanks to Richard Rood, Kevin Hamilton, and Noboru Nakamura for their helpful comments and discussions and to R. John Wilson for computational assistance in running SKYHI and viewing its output. One of us (SES) was funded for this work by NOAA grant NA26RG0102-01 to Princeton University.

References

Andrews, D. G., J. D. Mahlman, and R. W. Sinclair, Eliassen-Palm diagnostics of wave, mean-flow interaction in the GFDL 'SKYHI' general circulation model, *J. Atmos. Sci., 40*, 2768, 1983.

Barat, J., Some characteristics of clear air turbulence in the middle atmosphere, *J. Atmos. Sci., 39*, 2553, 1982.

Gage, K. S., and G. D. Nastrom, Theoretical interpretation of atmospheric wavenumber spectra of wind and temperature observed by commercial aircraft during GASP, *J. Atmos. Sci., 43*, 729, 1986.

Goldan, P. D., W. C. Kuster, D. L. Albritton, and A. L. Schmeltekopf, Stratospheric $CFCl_3$, CF_2Cl_2, and N_2O height profile measurements at several latitudes, *J. Geophys. Res., 85*, 413, 1980.

Loewenstein, M., J. R. Podolske, K. R. Chan, and S. E. Strahan, N_2O as a dynamical tracer in the Arctic vortex, *Geophys. Res. Lett., 17*, 477, 1990.

Mahlman, J. D., and L. J. Umscheid, Comprehensive modeling of the middle atmosphere: The influence of horizontal resolution, in *Transport Processes in the Middle Atmosphere*, edited by G. Visconti and R. Garcia, D. Reidel, Norwell, Mass., 1987.

Mahlman, J. D., H. Levy, II, and W. J. Moxim, Three-dimensional simulations of stratospheric N_2O: Predictions for other trace constituents, *J. Geophys. Res.*, *91*, 2687, 1986.

Nastrom, G. D., W. H. Jasperson, and K. S. Gage, Horizontal spectra of atmospheric tracers measured during the Global Atmospheric Sampling Program, *J. Geophys. Res.*, *91*, 13,201, 1986.

Podolske, J. R., M. Loewenstein, S. E. Strahan, and K. R. Chan, Stratospheric nitrous oxide distribution in the southern hemisphere, *J. Geophys. Res.*, *94*, 16,767, 1989.

Sato, T., and R. F. Woodman, Fine altitude resolution observations of stratospheric turbulent layers by the Arecibo 430 MHz radar, *J. Atmos. Sci.*, *39*, 2546, 1982.

Schoeberl, M. R., L. R. Lait, P. A. Newman, and J. E. Rosenfield, The structure of the polar vortex, *J. Geophys. Res.*, *97*, 7859, 1992.

Strahan, S. E., and J. D. Mahlman, Evaluation of the SKYHI general circulation model using aircraft N_2O measurements, 1, Polar winter stratospheric meteorology and tracer morphology, *J. Geophys. Res.*, this issue.

World Meteorological Organization (WMO), Atmospheric ozone, WMO Rep. 16, Global Ozone Res. and Monit. Proj., Geneva, 1986.

J. D. Mahlman, NOAA Geophysical Fluid Dynamics Laboratory, P.O. Box 308, Princeton, NJ 08542.

S. E. Strahan, NASA/Goddard, Mail Code 910.3, Greenbelt, MD 20771.

(Received September 2, 1992; revised November 1, 1993; accepted January 4, 1993.)